J Nanopart Res (2012) 14:979
DOI 10.1007/s11051-012-0979-1

RESEARCH PAPER

Stabilization of gold and silver nanowires inside cyclo[8]thiophene nanoaggregates: a theoretical study

Serguei Fomine

Received: 9 December 2011 / Accepted: 1 June 2012 / Published online: 22 June 2012

Abstract The stability and electronic properties of gold and silver nanowires (NWs) containing up to 12 atoms trapped inside cyclo[8]thiophenes (**CT8**) nanoaggregates have been modeled using M06 functional, 3-21G* basis set for nonmetallic atoms; LANL2DZ pseudopotential basis set for metals were applied for optimization; and 6-31G* and LANL2DZ basis sets for single point calculations, respectively. It has been found that the formation of (NW) inside **CT8** nanoaggregates is a thermodynamically favorable process and it could be a potentially useful method of metal NW stabilization. The inclusion of metal NW inside **CT8** nanoaggregates increases significantly the binding energy between macrocycles and changes the geometry of NW compared to that of free-standing clusters due to the size restriction imposed by the nanoaggregate cavity. The binding energies per metal atom reach a maximum for three metal atoms and then start decreasing with a possible stabilization for large NW. It was found that the binding energies between silver NW and **CT8** nanoaggregate are lower than those of gold NW and that in the case of gold NW containing more than four metal atoms the S0 → S1 excitation involves almost exclusively electrons of metal NW. On the other hand, in the case of silver NW the excitation involves the electron transfer from the NW to the **CT8** nanoaggregate.

Keywords Cyclothiophenes · Nanowires · DFT · Gold · Silver

S. Fomine (✉)
Instituto de Investigaciones en Materiales, Universidad Nacional Autónoma de México, Apartado Postal 70-360, CU, Coyoacán, 04510 Mexico, DF, Mexico
e-mail: fomine@servidor.unam.mx

Introduction

Molecular electronics have recently been recognized as one of the most viable alternatives for the future nanoscaled electronic devices (Kubatkin et al. 2003; Yu and Natelson 2004; Dadosh et al. 2005; Song et al. 2009). A great variety of potentially useful molecular electronic devices, such as molecular rectifiers, resonant tunneling diodes, wires, and storage devices have been designed and studied at both experimental and theoretical level (Tour 2000; Carroll and Gorman 2002; Seminario et al. 2000; Brandbyge et al. 2002; Soler et al. 2002; Taylor et al. 2001). Nanotubes (NTs) and nanowires (NWs) are among two important groups of so-called quasi-one-dimensional nanostructures. They have been considered as potential materials for nanoelectronic, nanolithography photocatalysis, microscopy, and other fields of modern nanotechnologies. The finite size effect causes drastic changes compared with bulk materials in structural, electronic, magnetic, and optical properties. However, the free-standing NWs become less stable as they get thinner

(Kondo and Takanayagi 2000). Therefore, enhancing the structural stability of NW is extremely important for their application. One of the stabilization approaches is NW filled inside carbon NTs, which has been studied both experimentally and theoretically (Ajayan and Iijima 1993; Grobert et al. 1999; Hsin et al. 2001; Hu et al. 2006). Thus, during the past few years, there have been fabricated nanocomposites based on NTs and NWs with a set of advanced properties (Hirsch and Vostrowsky 2005; Burghard 2005; Terrones et al. 2006; Ivanovskaya et al. 2005). For instance, carbon NT filled with such metals as Cr (Guerret-Piécourt et al. 1994), Fe (Grobert et al. 1999), Co (Leonhardt et al. 2003), Ni (Grobert et al. 1998), Cu (Setlur et al. 1996), and Ge (Loiseau and Pascard 1996) have been prepared. A variety of methods were used including arc-discharged method, chemical vapor deposition, and laser vaporization. In case of the metals having low melting point like Pb and Bi, the encapsulation is usually achieved by the contact of an open-capped NT in liquid phase and subsequent entering of the atoms into the NT cavity (Ajayan and Iijima 1993). As seen, all those methods are rather laborious involving filling the NTs by metal atoms in one or another way. This approach intrinsically leaves room for defects and incomplete filling. Those shortcomings might be avoided if the formation of a NT and a NW are simultaneous processes. It has been demonstrated recently that cyclooligothiophenes (CTs) are able to form stable columnar nanoaggregates due to π–π stacking interactions between CTs macrocycles (Flores et al. 2008) with the binding energy between macrocycles reaching more than 40 kcal/mol. Those macrocycles should be able to form inclusion complexes with metal ions when there is a match between the macrocycle cavity and the Van der Waals radius of a metal. The late transition metals are the best candidates to form inclusion complexes with CTs macrocycles due to their excellent affinity to sulfur. The reduction of the metallic ions which goes smoothly for late transition metals will lead to the formation of neutral inclusion complex able to self assemble to form a NW inside the NT. This process is schematically depicted in Fig. 1.

Therefore, the goal of this study is to validate the proposed method of NW stabilization using quantum

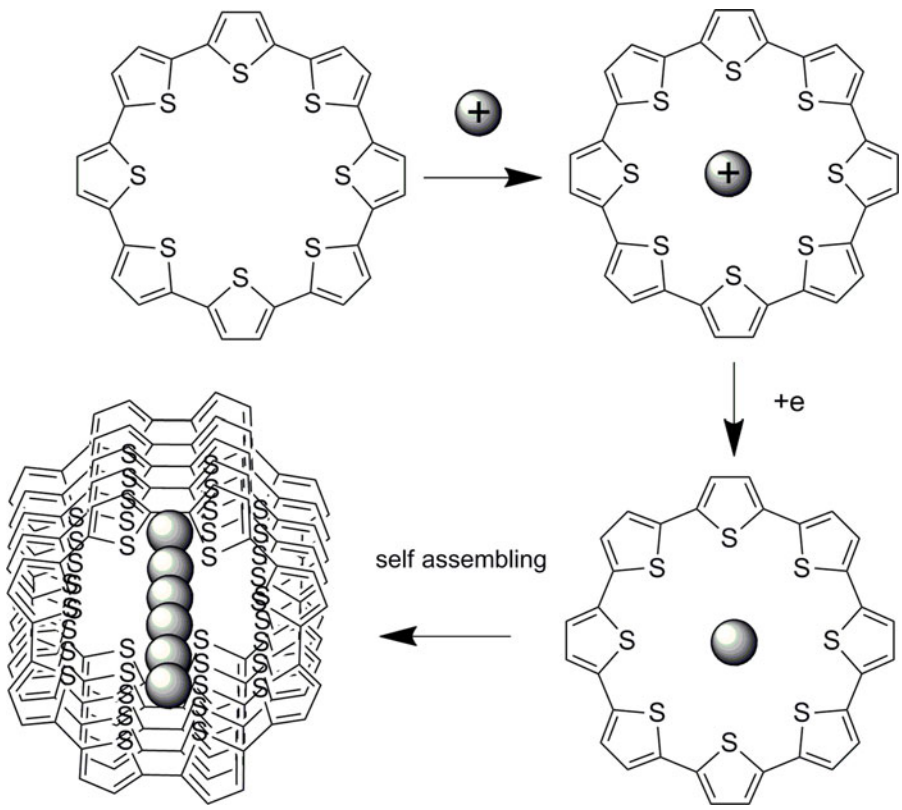

Fig. 1 CT-assisted formation of metallic NW inside CT nanoaggregate

chemistry tools. As a model CT macrocycle is taken where CT contains eight thiophene units (Fuhrmann et al. 2003) (**CT8**). **CT8** macrocycle has a diameter of internal cavity of around 4 Å. Good candidates to form neutral inclusion complex with **CT8** are gold and silver, having Van der Waals diameter of 3.32 and 3.44 Å, respectively. Therefore, the aim of this research is to explore theoretically the energetic of formation, structural and electronic properties of **Au** and **Ag** NW trapped inside the nanoaggregates formed by **CT8** macrocycles.

Computational details

All calculations were carried out using Gaussian 09 suit of programs (Frisch et al. 2009) with M06 (Zhao and Truhlar 2006) functional and 3-21G* basis set for all except metal atoms in case of geometry optimizations. Restricted and unrestricted formalisms were used for closed and open shell systems, respectively. No symmetry restrictions were imposed during the optimizations. LANL2DZ pseudopotential basis set was used to model gold and silver atoms of the NWs. M06 functional was shown to produce excellent results for weakly bounded and transition metal complexes, while 3-21G* basis set reproduces fairly well the geometry of oligothiophenes and weak interactions between CTs (Flores et al. 2008). M06/LANL2DZ model reproduces interatomic distances in $\mathbf{Au_2}$ and $\mathbf{Ag_2}$ molecules within 0.05 Å (Baetzold 1971). To improve the energy, single point calculations were carried out using LANL2DZ basis set for metals and 6-31G* one for nonmetals. This basis set is denominated as LACVP*. The excitation energies of NW-**CT8**-nanoaggregate complexes were estimated using time dependant implementation of CAM-B3LYP functional (Yanai et al. 2004) in combination with LACVP* basis set. This model reproduce well both the excitation energies of small **Au** and **Ag** clusters and **CT8**. Tubular aggregates of **CT8** and their inclusion complexes with NW are denoted as **nCT8** and **nCT8–mM**, respectively, where **n** is the number of **CT8** units in the aggregate and **m** is the number of atoms of metal **M** in the NW, respectively. The geometries of the lowest energy structures for **Au** and **Ag** clusters for the calculation of the binding energies were taken from Wang et al. (2002), Fournier (2001).

Results and discussion

Formation of tubular aggregates of **CT8**

The formation of tubular aggregates of **CT8** has been described in details earlier (Flores et al. 2008) at slightly different theoretical level (MPWB1K/3-21G* instead of M06/6-31G*//M06/3-21G* in this paper). Both the methods are consistent with one another. The binding energies between macrocycles calculated for dimer, trimer, tetramer, pentamer, and hexamer are very close for all tubular aggregated oscillating between 28 and 29 kcal/mol. As seen, the binding between macrocycles is strong enough to form stable tubular aggregates. For **3CT8**, **4CT8**, **5CT8**, and **6CT8** the binding energies represent average values. Previous work demonstrated (Flores et al. 2008) that the binding energy depends little on the position being slightly lower for central rings in nanoaggregate and, therefore, the average binding energy describes adequately the phenomenon of binding in the nanoaggregates. The minimal interplane distances between macrocycles in the nanoaggregates **3CT8**, **4CT8**, **5CT8**, and **6CT8** found for M06/3-21G* model is 3.3 Å, slightly larger compared to MPWB1K/3-21G* method (3.1 Å) and does not vary significantly with the size of nanoaggregate. The optimized structure of largest nanoaggregate **6CT8** is shown in Fig. 2.

Gold complexes

Figures 3, 4 and Table 1 show optimized geometries of the gold NW inside **CT8** nanoaggregates, total and partial density of states, and energetic characteristics of such complexes

CT8–Au

In case of the simplest model **CT8–Au**, the interaction of the gold atom with macrocycle **CT8** achieves 12.2 kcal/mol. The distances between **S** and **Au** atoms in the complex are 3.70 and 4.04 Å, depending on the thiophene fragment position. This distance is somewhat larger than the sum of Van der Waals radii of **S** and **Au** atoms suggesting that the interaction is mainly nonbonded by nature. TDDFT calculations demonstrated that the first allowed transition for **CT8–Au** is at 2.73 eV (S0 → S12). The natural transition orbitals (NTOs) (Martin 2003) for this transition are

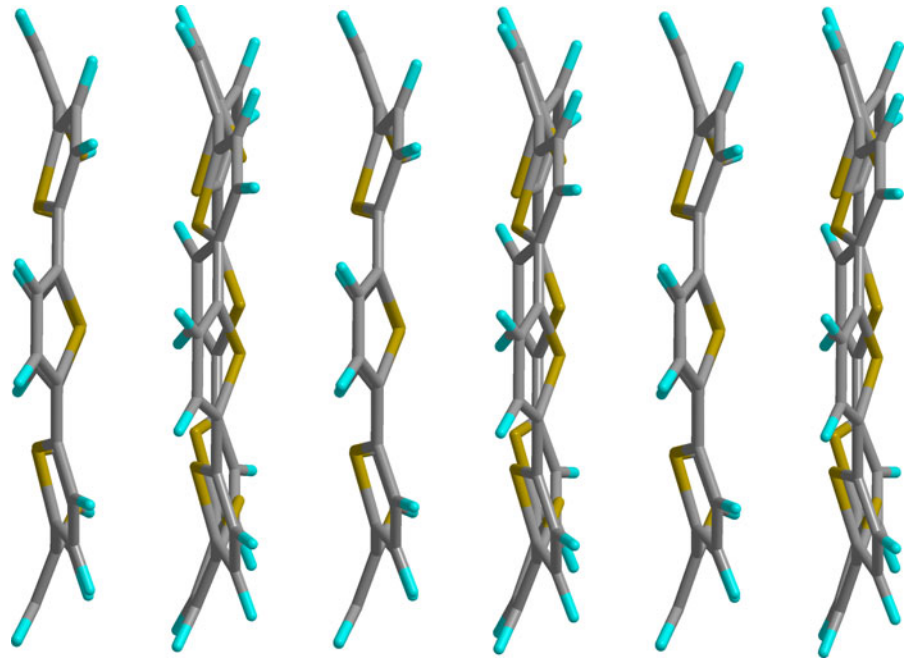

Fig. 2 M06/3-21G*-optimized geometry of **6CT8**

shown in Fig. 7. As seen, this transition involves only π-electrons of **CT8** macrocycle without affecting the **Au** atom.

2CT8–2Au

In the case of dimer **2CT8–2Au**, the interaction energy between **Au** dimer and **2CT8** nanoaggregate is about twice as high as for **CT8**–**Au** (Table 1). Neither the interplane distance between thiophene fragments in **2CT8–2Au** nor the **Au**–**Au** distance change significantly compared to free-standing nanoaggregate and $\mathbf{Au_2}$ cluster, being 3.3 and 2.60 Å, respectively. The binding energy between **CT8–Au** fragments in **2CT8–2Au** increased to 77.5 kcal/mol, compared to 28.8 kcal/mol for free macrocycles due to additional binding between **Au** atoms. The first allowed excited state for **2CT8–2Au** is S1 with the energy of 2.67 eV due to lower symmetry. Unlike **CT8–Au**, there is electron transfer from macrocycles to the gold atoms during the excitation (Fig. 7).

3CT8–3Au

Unlike monomer and dimer where **Au** atoms lay in the macrocycle plane, in **3CT8–3Au** **Au** atoms lie between planes forming a triangle of approximate C_{2v} symmetry. The binding energy between $\mathbf{Au_3}$ cluster and **3CT8** nanoaggregate increases to 51.5 kcal/mol, more than four times higher than that between **Au** and **CT8** in **CT8–Au**. The increase of the binding energy is due to smaller **S**–**Au** distance for two gold atoms at the base of triangle achieving 2.80 Å. While the interplane distances between thiophene fragments are not affected by the incorporation of three gold atoms, the complexation does affect the distances between **Au** atoms: they increase by 0.04–0.05 Å compared to free $\mathbf{Au_3}$ cluster. Similar to **2CT8–2Au**, the binding energy between **CT8–Au** fragments is more than twice as high as that for free-standing nanoaggregate **3CT8** due to additional binding from $\mathbf{Au_3}$ cluster. Similar to dimer, the S0 → S1 transition involves both gold and macrocycle atoms showing charge transfer from $\mathbf{Au_3}$ cluster to the macrocycle (Fig. 7).

4CT8–4Au

The lowest energy configuration of $\mathbf{Au_4}$ cluster and that forming inclusion complex with **4CT8** nanoaggregate have the same rhombic structure. The **Au**–**Au** distances of the gold tetramer inside **4CT8**

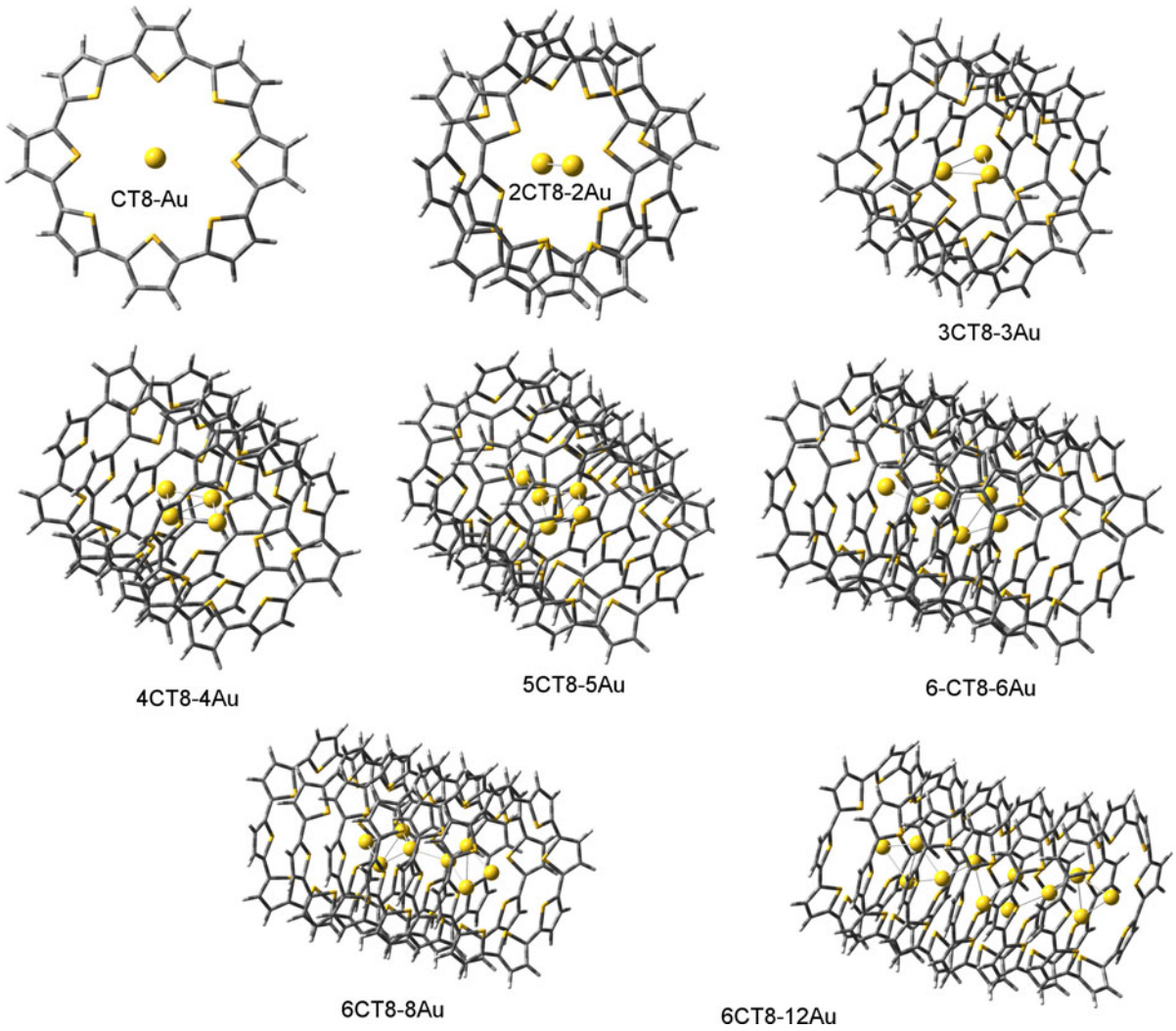

Fig. 3 Optimized geometries of gold NW inside of tubular aggregates of **CT8**

nanoaggregate is 0.04–0.05 Å larger than those in the tetramer alone to adjust the distances between **S** and **Au** atoms, similar to **3CT8–3Au**. On the other hand, a shortening of interplane distances between thiophene fragments to 3.25–3.27 Å was observed. The binding energy between gold tetramer and **4CT8** increases to 54.7 kcal/mol, while the average binding energy between **CT8–Au** fragments remains almost constant (72.8 kcal/mol, Table 1). Similar to **3CT8–3Au** the gold atoms are located between macrocycles interacting with two adjacent cyclic fragments. The lowest allowed electron transition for **4CT8–4Au** is S0 → S1 located at 1.91 eV. As can be seen from the Fig. 7, there is only weak charge transfer from the gold atoms to the macrocycles.

5CT8–5Au

Unlike previous complexes where the lowest energy configuration of $\mathbf{Au_n}$ free-standing cluster and that inside the nanoaggregate has been the same, starting from **5CT8–5Au** those structures are different due to geometric restriction imposed by the NT cavity. As seen from the Fig. 3 the $\mathbf{Au_5}$ cluster inside the NT is a rhomb containing four **Au** atoms with fifth atom located almost at the axis of a nanoaggregate. On the

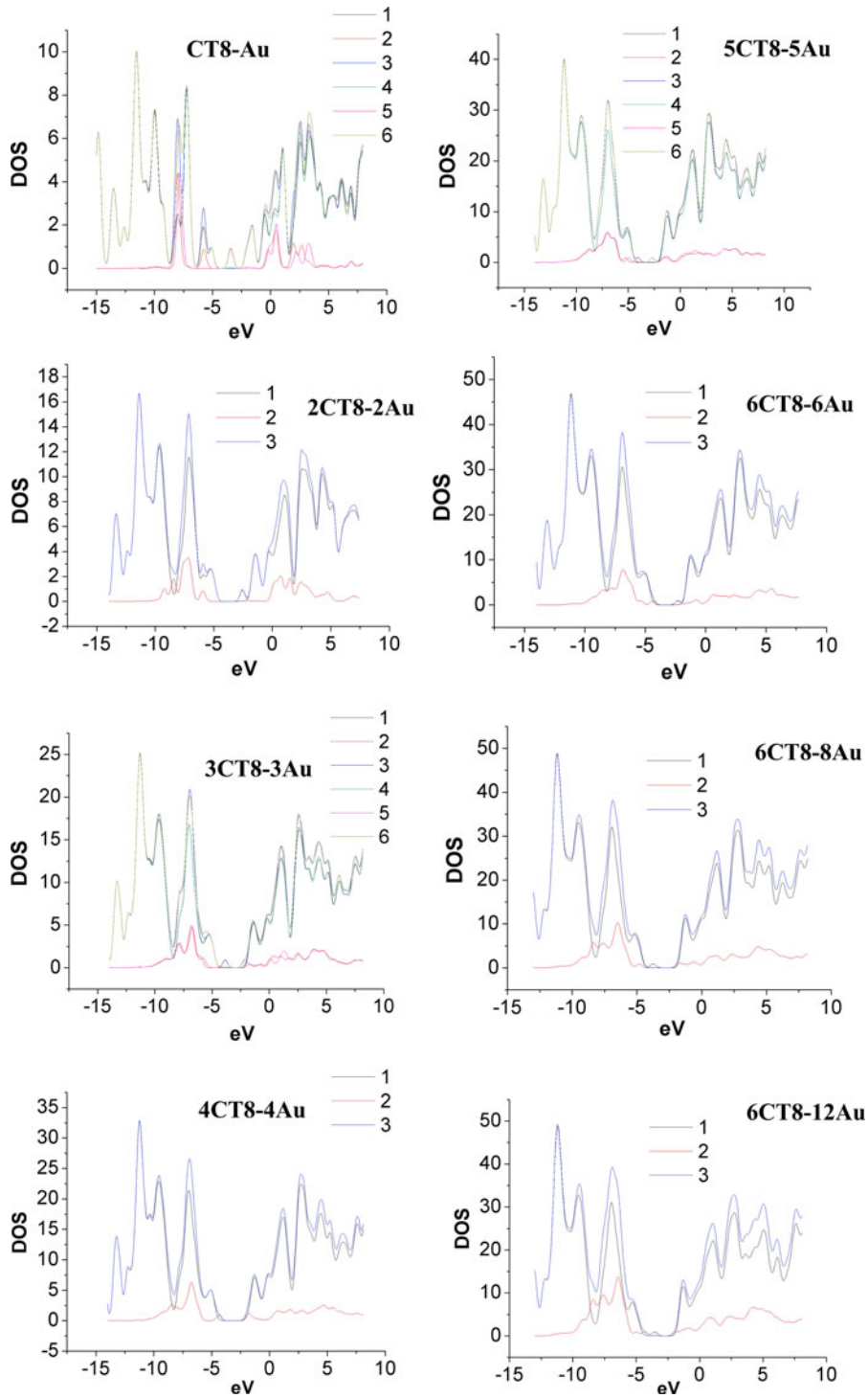

Fig. 4 Density of states (DOS). For open shell systems; **nCT8–mAu** ($\mathbf{n} = \mathbf{m} = 1, 3$ and 5): *1* contribution of **nCT8** to DOS (α-spin orbitals), *2* contribution of $\mathbf{Au_n}$ to DOS (α-spin orbitals), *3* total DOS (α-spin orbitals), *4* contribution of **nCT8** to DOS (β-spin orbitals), *5* contribution of $\mathbf{Au_n}$ to DOS (β-spin orbitals), *6* total DOS (β-spin orbitals). For closed shell systems; **nCT8–mAu** ($\mathbf{n} = \mathbf{m} = 2, 4, 6$ and $\mathbf{n} = 6$, $\mathbf{m} = 8$ and 12) **1**-contribution of **nCT8** to DOS, **2**-contribution of $\mathbf{Au_n}$ to DOS, **3**-total DOS

other hand, the standalone lowest energy $\mathbf{Au_5}$ cluster has flat trapezoidal C_{2v} structure. The geometry of $\mathbf{Au_5}$ cluster is changed inside the nanoaggregate to maximize the interaction energy which is 55.4 kcal/mol. This is about five times higher than the interaction energy of a single **Au** atom with **CT8** macrocycle. For the complexes of **Au** clusters with **CT8** nanoaggregates where the geometry of **Au** cluster inside the

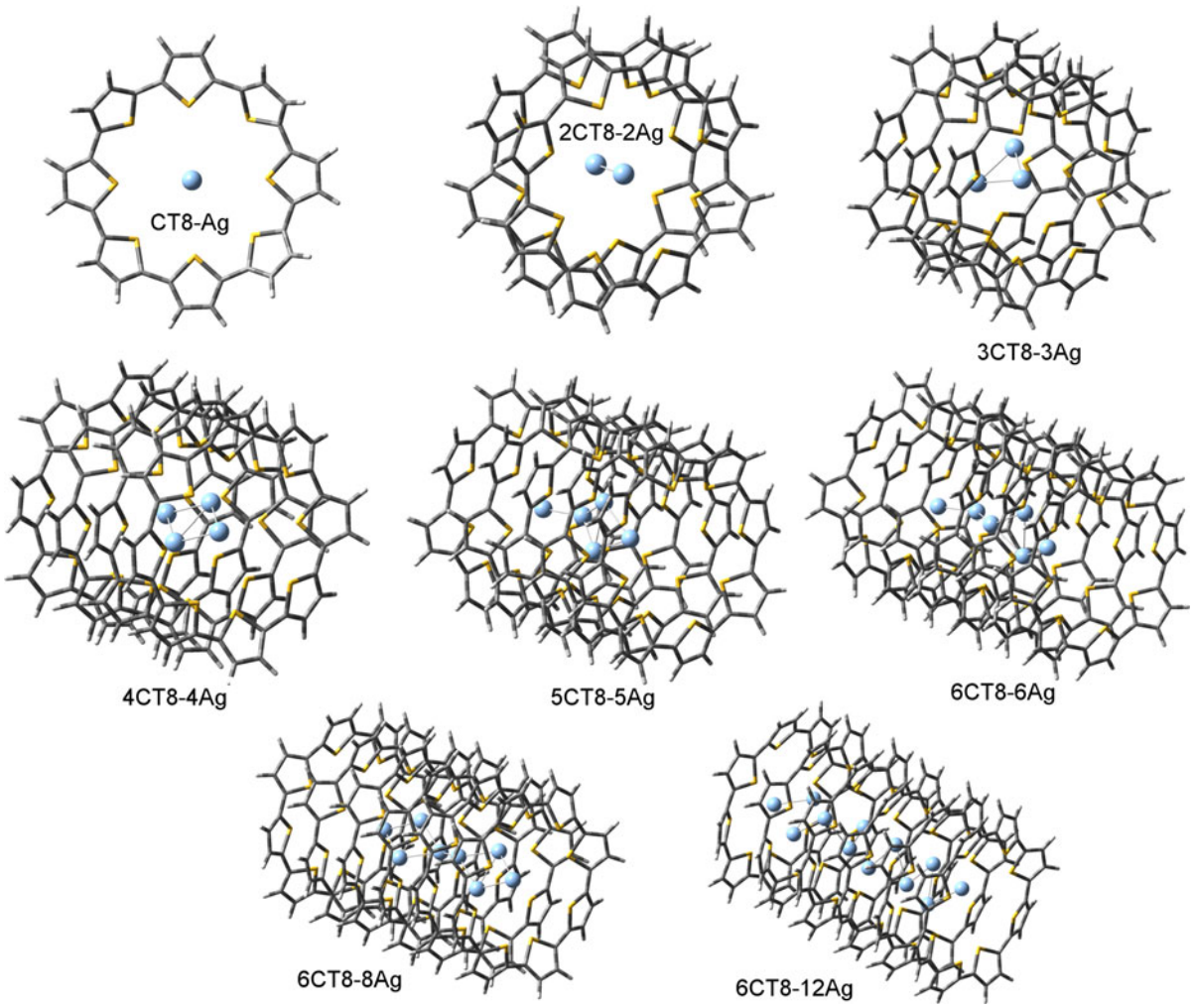

Fig. 5 Optimized geometries of silver NW inside of tubular aggregates of **CT8**

nanoaggregate is different from that of the lowest energy free-standing isomer, the estimated binding energy between **Au** cluster and a nanoaggregate is calculated using the lowest energy free-standing isomer. Even in this case the resulting binding energy is high, reflecting the stability of the complexes. As can be seen from the analysis of NTOs for S0 → S1 transition of **5CT8–5Au** (Table 1; Fig. 7) involves almost exclusively the orbitals of $\mathbf{Au_5}$ cluster, leaving intact the macrocycles.

6CT8–6Au

The geometry of $\mathbf{Au_6}$ cluster inside the **6CT8** nanoaggregate is a rhomb with two extra atoms located almost at the axes of the **6CT8** unlike plane D_{3h}, the lowest energy standalone isomer of $\mathbf{Au_6}$. The interaction energy between NT and the cluster decreases to 42.8 kcal/mol. As seen from the Fig. 3, the $\mathbf{Au_6}$ cluster inside **6CT8** nanoaggregate is shorter compared to **6CT8** so that the interaction occurs mostly with four inner macrocycles and, therefore, **6CT8** is able to accommodate more gold atoms. Similar to **5CT8–5Au**, S0 → S1 excitation involves only $\mathbf{Au_6}$ without involving orbitals of nanoaggregate (Fig. 7).

6CT8–8Au and 6CT8–12Au

As it has been shown above, **6CT8** has enough room to accommodate more than 6 gold atoms. Thus,

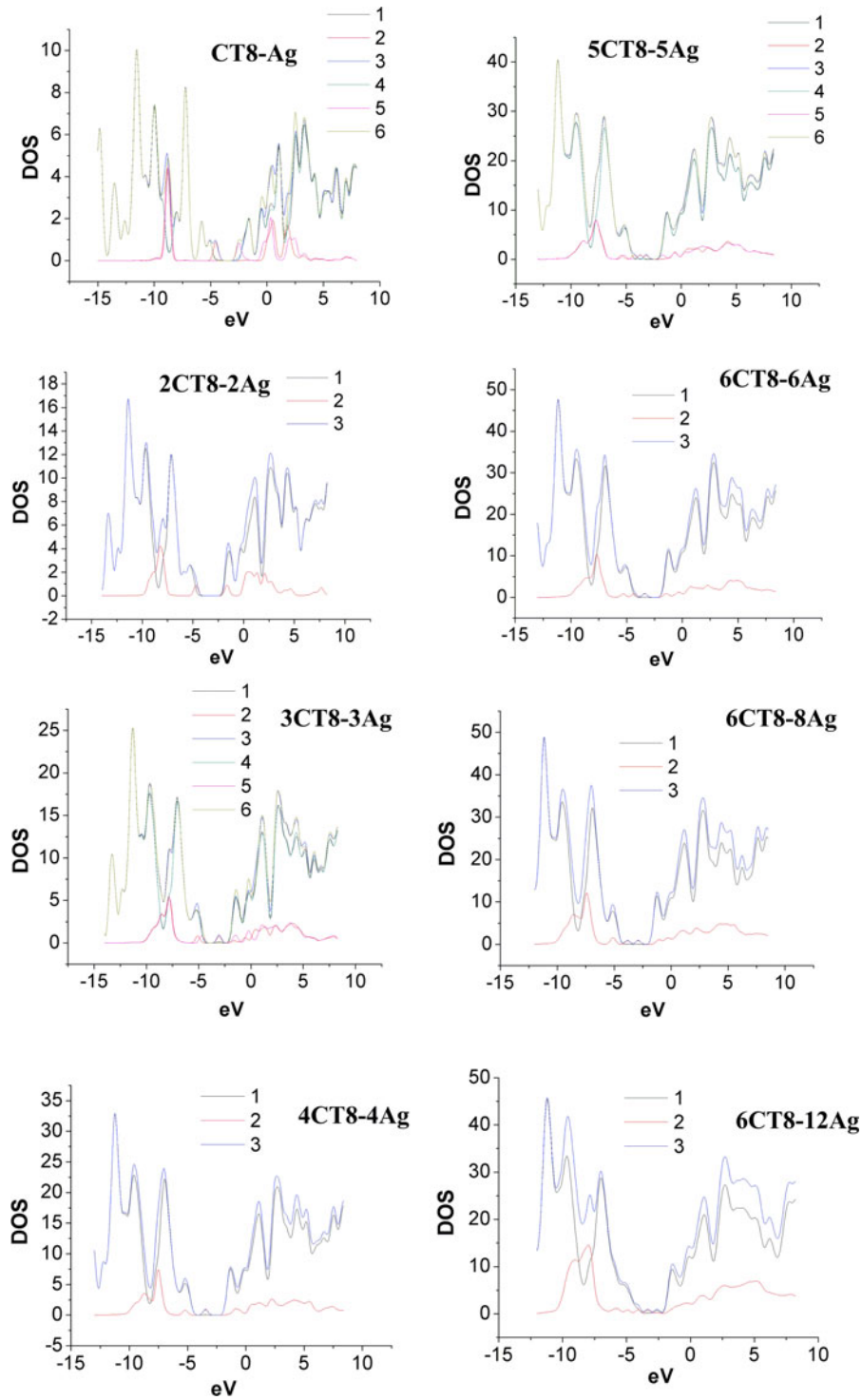

Fig. 6 Density of states (DOS). For open shell systems; **nCT8–mAg** ($\mathbf{n} = \mathbf{m} = 1$, 3 and 5): *1* contribution of **nCT8** to DOS (α-spin orbitals), *2* contribution of $\mathbf{Ag_n}$ to DOS (α-spin orbitals), *3* total DOS (α-spin orbitals), *4* contribution of **nCT8** to DOS (β-spin orbitals), *5* contribution of $\mathbf{Ag_n}$ to DOS (β-spin orbitals), *6* total DOS (β-spin orbitals). For closed shell systems; **nCT8–mAg** ($\mathbf{n} = \mathbf{m} = 2$, 4, 6 and $\mathbf{n} = 6$, $\mathbf{m} = 8$ and 12) **1**-contribution of **nCT8** to DOS, **2**-contribution of $\mathbf{Ag_n}$ to DOS, **3**-total DOS

6CT8–8Au has $\mathbf{Au_8}$ NW in the form of two interconnected rhombs while standalone lowest energy $\mathbf{Au_8}$ cluster is a structure possessing T_d symmetry. The binding energy between **6CT8** and $\mathbf{Au_8}$ reaches 54.0 kcal/mol and S0 → S1 excitation energy slightly decreases compared to **6CT8–6Au** (1.93 vs 1.98 eV).

Table 1 Calculated S0 → S1 energies (eV), binding energies ($\mathbf{E_{b1}}$ and $\mathbf{E_{b2}}$, kcal/mol), and charge (Q) on metal NW for NW-tubular nanoaggregate complexes

Complex	S0 → S1	$\mathbf{E^b_{b1}}$	$\mathbf{E^c_{b2}}$	Q^d
CT8–Au	2.7312[a]	–	12.2	−0.09
2CT8–2Au	2.67	77.5	25.3 (12.6)	−0.46 (−0.23)
3CT8–3Au	1.52	71.5	51.5 (17.2)	−0.95 (−0.32)
4CT8–4Au	1.91	72.8	54.7 (13.7)	−1.38 (−0.35)
5CT8–5Au	1.51	70.5	55.4 (11.1)	−1.72 (−0.34)
6CT8–6Au	1.98	70.5	42.8 (7.1)	−2.07 (−0.35)
6CT8–8Au	1.93	–	54.0 (6.7)	−2.66 (−0.33)
6CT8–12Au	1.36	–	43.2 (3.6)	−3.57 (0.30)
CT8–Ag	2.28[a]	–	10.8	−0.07
2CT8–2Ag	2.70	71.2	21.4 (10.7)	−0.44 (−0.22)
3CT8–3Ag	1.17	67.8	47.6 (15.9)	−0.84 (0.28)
4CT8–4Ag	1.57	68.2	50.6 (12.7)	−1.29 (−0.32)
5CT8–5Ag	1.30	65.8	49.4 (9.9)	−1.61 (−0.32)
6CT8–6Ag	1.65	65.2	38.0 (6.3)	−1.97 (−0.33)
6CT8–8Ag	1.22	–	34.8 (4.4)	−2.50 (−0.31)
6CT8–12Ag	0.53	–	25.5 (2.1)	−1.84 (−0.15)

[a] S1 → S12 and S1 → S4 energies for **CT8–Au** and **CT8–Au** complexes, respectively

[b] The total electronic energy difference of the complexes **nCT8–nM** and a sum of total electronic energies of **n** complexes **CT8–M**

[c] The total electronic energy difference of **nCT8–mM** complex and a sum of total electronic energies of **nCT8** and the lowest energy configuration of **mM** cluster. Values in brackets are per metal atom

[d] Values in brackets are per metal atom

As seen from the Fig. 7 only orbitals of $\mathbf{Au_8}$ are involved to the excitation. The **Au**–**Au** distances in rhombic fragments of $\mathbf{Au_8}$ are close to those found for **4CT8–4Au** (2.82–2.85 Å). The **Au**–**Au** distance between two rhombs is of 2.71 Å.

The largest complex **6CT8–12Au** has the binding energy of 43.2 kcal/mol and the smallest S0 → S1 excitation energy among all complexes (1.36 eV). The standalone $\mathbf{Au_{12}}$ cluster is a C_s structure. As seen from the analysis of NTO orbitals, the excitation involves mostly $\mathbf{Au_{12}}$ NW. The geometry of $\mathbf{Au_{12}}$ inside **6CT8** nanoaggregate is a zigzag structure of 1.77 nm length, almost exactly the length of **6CT8** nanoaggregate. The interplane distance between **CT8** macrocycles maintains around 3.3 Å, similar to free **6CT8**.

Summary

The formation of **nCT8–nAu** complexes starting either from **nCT8** and **nAu** or from **CT8–Au** complex is a thermodynamically favorable process as seen from the Table 1. Therefore, those complexes might probably be formed by self-assembling. The geometry of the lowest energy standalone $\mathbf{Au_n}$ isomers and those inside **nCT8** nanoaggregates are similar up to $\mathbf{n} = 4$, for larger clusters their geometry are different due to the restrictions imposed by the nanoaggregate cavity. The absolute binding energy between **nCT8** and **mAu** increases with **m** to pentamer and then starts decreasing, while the binding energy per **Au** atom increases from $\mathbf{m} = 1$ to $\mathbf{m} = 3$) and then decreases too with possible tendency to stabilize for larger systems. The NBO charges at **Au** NW inside **nCT8** nanoaggregate become more negative with size of NW (Table 1). This is due to favoring the charge transfer interaction between metal cluster and organic nanoaggregates. Thus, HOMO increases its energy from −5.10 to −4.69 eV going from **CT8** to **6CT8**, while LUMO of **Au** clusters decreases its energy from −3.34 for **Au** atom to −3.87 eV for $\mathbf{Au_{12}}$ cluster, thus promoting the charge transfer from nanoaggregate to **Au** atoms for large clusters.

The lowest allowed excitation energies are S0 → S1 for all but **CT8–Au** complex. They tend to

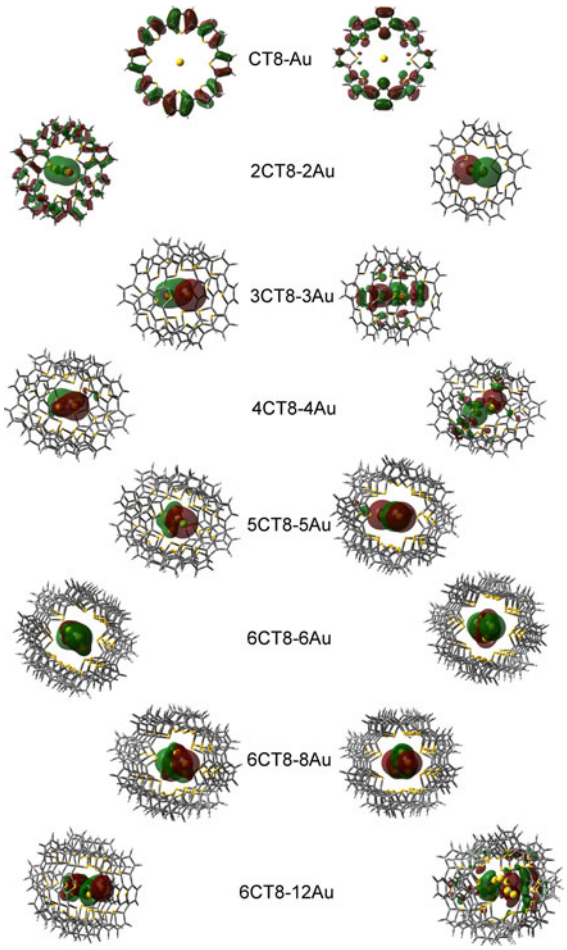

Fig. 7 The dominant NTO pairs for the first allowed transition in gold NW-tubular aggregates complexes calculated at CAM-B3LYP/LACVP* level. The "hole" is on the *left*, the "particle" on the *right*

decrease with **m** and starting from **4CT8–4Au** complex, the excitation involves almost exclusively electrons of metal NW.

Silver complexes

Due to similarity of the electronic structure and Van der Waals radii of gold and silver atoms, the structural, energetic, and electronic features of gold and silver complexes with **nCT8** nanoaggregates are very much alike. Therefore, we will focus mostly on the differences between gold and silver complexes in this section. Figure 6 shows total and partial density of states of **nCT8–mAg** complexes. As seen from the Fig. 5, the geometry of $\mathbf{Ag_n}$ clusters inside **nCT8** nanoaggregates is very similar to **Au** clusters. The metal–metal distances are 0.02–0.03 Å shorter in the case of **Ag** NW. As seen from the Table 1, both $\mathbf{E_{b1}}$ and $\mathbf{E_{b2}}$ binding energies are slightly lower for silver clusters. The difference in $\mathbf{E_{b1}}$ is related with stronger **Au–Au** bond (Verhaegen et al. 1962) compared to **Ag–Ag** one, while higher $\mathbf{E_{b2}}$ for **Au** complexes is related with higher electronegativity of **Au** atoms compared to **Ag** ones, which is reflected in more negative charges at **Au** atoms compared to **Ag** ones. For the clusters with the same number of atoms, the LUMO energies are lower for **Au** cluster resulting in better interactions with occupied orbitals of **nCT8** nanoaggregates. This effect can be noted examining NBO charges at metal atoms for the complexes. As seen, the charges are always more negative for **Au**-containing systems (Table 1) suggesting more efficient orbital interactions. On the other hand, similarly to **nCT8–mAu** the negative charge on **Ag** cluster increases with size. This phenomenon reflects increase of HOMO energy with the size of the clusters, thus facilitating the back donation from metal to **nCT8** nanoaggregate.

As seen from the Table 1, the lowest allowed excitation energies are lower for **Ag**-containing systems except for **2CT8–2M**, where excitation energies are slightly higher for **2CT8–2Ag** (2.67 vs 2.70 eV). Similarly to **CT8–Au**, the first allowed transition in **CT8–Ag** is not S0–S1 one due to symmetry reasons. Unlike gold-containing systems where starting from **4CT8–4Au** complex the excitation involves almost exclusively electrons of metal NW; in the case of **nCT8–mAg** complexes, the excitation involves the electron transfer from the NW to the **nCT8** nanoaggregate (Fig. 8). This transfer is almost complete in the case of complexes having even number of the **Ag** atoms starting from **4CT8–4Ag**.

The difference between two metals is also related to higher electronegativity of **Au** compared to **Ag**. In case of **Ag**-containing systems, low-lying unoccupied orbitals of **nCT8** are close in energy to those involving **Ag** NW, resulting in mixing of orbitals belonging to **Ag** NW and **nCT8** nanoaggregate in the first excited state. On the other hand, in the case of **Au**-containing systems, the energy difference between those orbitals is too large; therefore, unoccupied orbitals of **nCT8** nanoaggregate do not participate significantly in the first excited state. Thus, in case of **2CT8–2Au** complex, the highest occupied and the lowest

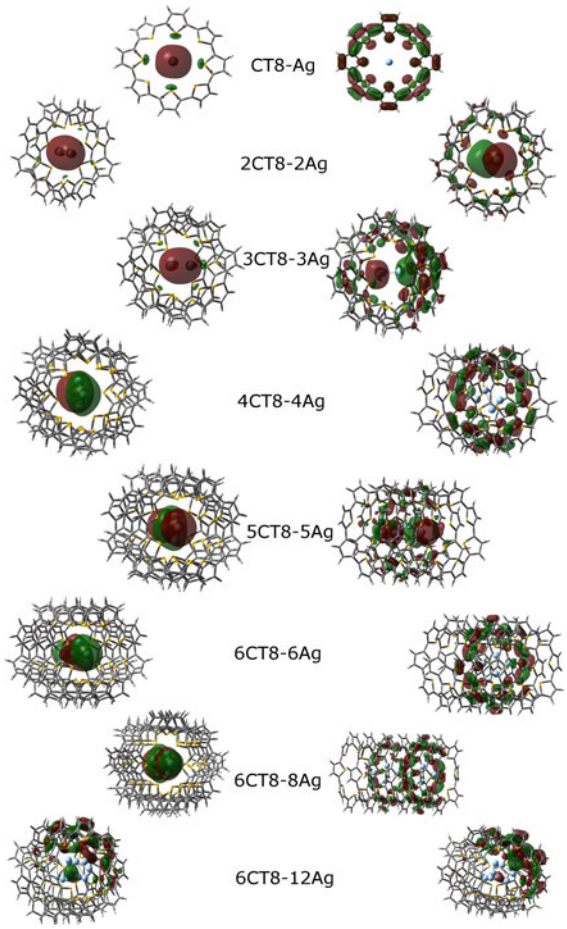

Fig. 8 The dominant NTO pairs for the first allowed transition in silver NW-tubular aggregates complexes estimated at CAM-B3LYP/LACVP* level. The "hole" is on the *left*, the "particle" on the *right*

unoccupied orbitals involving metal atoms are HOMO−6 (−5.95 eV) and LUMO (−2.55 eV), respectively, while for **2CT8–2Ag** complex those orbitals are HOMO (−4.72 eV) and LUMO+1 (−1.67 eV), respectively. In the case of **2CT8–2Au**, the most important contribution to S0 → S1 transition is HOMO–LUMO excitation. Therefore, $\mathbf{Au_2}$ cluster receives electron on excitation (Fig. 7). On the other hand, the same HOMO–LUMO transition, which also has an important contribution to S0–S1 excitation leads to the electron transfer from $\mathbf{Ag_2}$ cluster to the **2CT8** nanoaggregate, since the most important contribution to LUMO of **2CT8–2Ag** comes from π orbitals of **2CT8** nanoaggregate.

Conclusions

The formation of NW of gold and silver inside **nCT8** nanoaggregates is a thermodynamically favorable process and it could be a potentially useful method of metal NW stabilization. The formation of inclusion metal complexes increases significantly the binding energy between macrocycles and changes the geometry of NW compared to that for the free-standing clusters due to size restriction imposed by the nanoaggregate cavity starting from cluster with five metal atoms. The binding energies between metal NW and **nCT8** nanoaggregate increase continuously with the number of metal atoms for both the metals to tetramer or pentamer and then tend to deline with possible stabilization for large NW. The bonding between **nCT8** and **Ag** clusters is notoriously weaker compared to **Au** ones. There are two consequences of higher gold atoms electronegativity compared to silver. The first one is that binding energies between silver NW and **nCT8** nanoaggregate are slightly lower than those of gold NW and the second one is that in case of gold-containing systems starting from **4CT8–4Au** complex, the excitation involves almost exclusively electrons of metal NW while in the case of **nCT8–mAg** complexes, the excitation involves the electron transfer from the NW to the **nCT8** nanoaggregate (Fig. 8). This transfer is almost complete in the case of complexes having even number of the **Ag** atoms starting from **4CT8–4Ag**. The lowest energy allowed excitation energies were estimated for **6CT8–12Ag** and **6CT8–12Au**, of 0.53 and 1.36 eV, respectively.

Acknowledgments The authors acknowledge the financial support from CONACYT Mexico (Grant 151277).

References

Ajayan PM, Iijima S (1993) Capillarity-induced filling of carbon nanotubes. Nature 361:333–334. doi:10.1038/361333a0

Baetzold RC (1971) Calculated properties of metal aggregates. I. Diatomic molecules. J Chem Phys 55:4355–4363. doi:10.1063/1.1676760

Brandbyge M, Mozos J-L, Ordejón P, Taylor J, Stokbro K (2002) Density-functional method for nonequilibrium electron transport. Phys Rev B 65:165401. doi:10.1103/PhysRevB.65.165401

Burghard M (2005) Electronic and vibrational properties of chemically modified single-wall carbon nanotubes. Surf Sci Rep 58:1–109. doi:10.1016/j.surfrep.2005.07.001

Carroll RL, Gorman CB (2002) The genesis of molecular electronics. Angew Chem Int Ed 41:4378–4400. doi:10.1002/1521-3773(20021202)41:23

Dadosh T, Gordin Y, Krahne R, Khivrich I, Mahalu D, Frydman V, Sperling J, Yacoby A, Bar-Joseph I (2005) Measurement of the conductance of single conjugated molecules. Nature 436:677–680. doi:10.1038/nature03898

Flores P, Guadarrama P, Ramos E, Fomine S (2008) Tubular aggregates of cyclic oligothiophenes. A theoretical study. J Phys Chem A 112:3996–4003. doi:10.1021/jp710654k

Fournier R (2001) Theoretical study of the structure of silver clusters. J Chem Phys 115:2165–2177. doi:10.1063/1.1383288

Frisch MJ et al (2009) Gaussian 09, revision B.01. Gaussian, Inc., Wallingford

Fuhrmann G, Debaerdemaeker T, Bäuerle P (2003) C–C bond formation through oxidatively induced elimination of platinum complexes—a novel approach towards conjugated macrocycles. Chem Commun 948–949. doi:10.1039/B300542A

Grobert N, Terrones M, Osborne AJ, Terrones H, Hsu WK, Trasobares S, Zhu YQ, Hare JP, Kroto HW, Walton RM (1998) Thermolysis of C60 thin films yields Ni-filled tapered nanotubes. Appl Phys A 67:595–598

Grobert N, Hsu WK, Zhu YQ, Hare JP, Kroto HW, Walton DRM, Terrones M, Terrones H, Redlich Ph, Rühle M, Escudero R, Morales F (1999) Enhanced magnetic coercivities in Fe nanowires. Appl Phys Lett 75:3363–3365. doi:10.1063/1.125352

Guerret-Piécourt C, Le Bouar Y, Loiseau A, Pascard H (1994) Relation between metal electronic structure and morphology of metal compounds inside carbon nanotubes. Nature 372:761–765. doi:10.1038/372761a0

Hirsch A, Vostrowsky O (2005) Functionalization of carbon nanotubes top. Curr Chem 245:193–237. doi:10.1007/b98169

Hsin YL, Hwang KC, Chen FR, Kai JJ (2001) Production and in situ metal filling of carbon nanotubes in water. Adv Mater 13:830–833. doi:10.1002/1521-4095(200106)13:11

Hu J, Bando Y, Zhan J, Zhi C, Golberg D (2006) Carbon nanotubes as nanoreactors for fabrication of single-crystalline Mg_3N_2 nanowires. Nano Lett 6:1136–1140. doi:10.1021/nl060245v

Ivanovskaya VV, Makurin YuN, Ivanovskii AL (2005) Fullerene peapods and related nanomaterials: synthesis, structure and electronic structure. In: Diudea M (ed) Nanostructures: novel architectures. Nova Science Publishers, New York, pp 9–24

Kondo Y, Takayanagi K (2000) Synthesis and characterization of helical multi-shell gold nanowires. Science 289:606–608. doi:10.1126/science.289.5479.606

Kubatkin S, Danilov A, Hjort M, Cornil J, Brédas J-L, Stuhr-Hansen N, Hedegård P, Bjórnholm T (2003) Single-electron transistor of a single organic molecule with access to several redox states. Nature 425:698–701. doi:10.1038/nature02010

Leonhardt A, Ritschel A, Kozhuharova R, Graff A, Mühl T, Huhle R, Mönch I, Elefant D, Schneider CM (2003) Synthesis and properties of filled carbon nanotubes. Diam Relat Mater 12:790–793. doi:10.1016/S0925-9635(02)00325-4

Loiseau A, Pascard H (1996) Synthesis of long carbon nanotubes filled with Se, S, Sb and Ge by the arc method. Chem Phys Lett 256:246–252

Martin RL (2003) Natural transition orbitals. J Chem Phys 118:4775–4777. doi:10.1063/1.1558471

Seminario JM, Zacarias AG, Tour JM (2000) Theoretical study of a molecular resonant tunneling diode. J Am Chem Soc 122:3015–3020. doi:10.1021/ja992936h

Setlur AA, Lauerhaas JM, Dai JY, Chang RPH (1996) A method for synthesizing large quantities of carbon nanotubes and encapsulated copper nanowires. Appl Phys Lett 69:345–347. doi:10.1063/1.118055

Soler JM, Artacho E, Gale JD, García A, Junquera J, Ordejón P, Sánchez-Portal D (2002) The SIESTA method for *ab initio* order—*N* materials simulation. J Phys Condens Matter 14:2745–2779. doi:10.1088/0953-8984/14/11/302

Song H, Kim Y, Jang YH, Jeong H, Reed MA, Lee T (2009) Observation of molecular orbital gating. Nature 462:1039–1043. doi:10.1038/nature08639

Taylor J, Guo H, Wang J (2001) *Ab initio* modeling of quantum transport properties of molecular electronic devices. Phys Rev B 63:245407. doi:10.1103/PhysRevB.63.245407

Terrones H, Lopez-Urias F, Munoz-Sandoval E, Rodriguez-Manzo JA, Zamudio A, Elias AL, Terrones M (2006) Magnetism in Fe-based and carbon nanostructures: theory and applications. Solid State Sci 8:303–320

Tour JM (2000) Molecular electronics. Synthesis and testing of components. Acc Chem Res 33:791–804. doi:10.1021/ar0000612

Verhaegen G, Stafford FE, Goldfinger P, Ackerman M (1962) Correlation of dissociation energies of gaseous molecules and of heats of vaporization of solids. Part 1.—Homonuclear diatomic molecules. Trans Faraday Soc 58:1926–1938. doi:10.1039/TF9625801926

Wang J, Wang G, Zhao J (2002) Density-functional study of Au_n ($n = 2$–20) clusters: lowest-energy structures and electronic properties. Phys Rev B 66:035418. doi:10.1103/PhysRevB.66.035418

Yanai T, Tew D, Handy N (2004) A new hybrid exchange–correlation functional using the Coulomb-attenuating method (CAM-B3LYP). Chem Phys Lett 393:51–57. doi:10.1016/j.cplett.2004.06.011

Yu LH, Natelson D (2004) The Kondo effect in C_{60} single-molecule transistors. Nano Lett 4:79–83. doi:10.1021/nl034893f

Zhao Y, Truhlar DG (2006) A new local density functional for main-group thermochemistry, transition metal bonding, thermochemical kinetics, and noncovalent interactions. J Chem Phys 125:194101. doi:10.1063/1.2370993